

UNIVERSITY OF TWENTE.

Faculty of Science and Technology
Chemical Engineering
Soft Matter, Fluidics and Interfaces

Fabrication and characterization of patterned titania layers

A thesis submitted for the degree of Master of Science

Erilia Yusnitha

Examination Committee:

Prof. Dr. Ir. R.G.H Lammertink

Prof. Dr. G. Mul

Aura Visan, MSc.

Renée Ripken, MSc.

29 August 2017

Abstract

The report presents two main parts, which are fabrication of TiO₂ layer on microchannel silicon substrate and characterization of photocatalytic performance of TiO₂ layer. The catalyst deposition on the substrate was conducted by using washcoating techniques. The morphology of catalyst layer obtained was analyzed by using SEM. The adhesion test was conducted to observe the adherence of catalyst layer to the substrate. SEM was used to observe the difference of catalyst layer between before and after adhesion test. The photocatalytic performance of catalyst layers was investigated by determining the intrinsic surface reaction rate constant. In order to determine the intrinsic surface reaction rate constant the results from numerical simulation were fitted to experimental data obtained for various residence times, substrate types and pH solution.

Table of Contents

Abstract	2
Chapter 1. General Introduction	4
1.1. Introduction.....	4
1.2. Photocatalysis.....	4
1.3. Photocatalysts	6
1.4. Semiconductors	7
1.5. Methylene blue	8
Chapter 2. Scope of Research.....	9
Chapter 3. Fabrication of the TiO ₂ catalyst layer.....	10
3.1. Introduction.....	10
3.2. Catalyst deposition experiment	10
3.2.1. Material preparation	10
3.2.2. Substrate and PDMS preparation.....	11
3.2.3. Catalyst deposition on flat silicon.....	11
3.2.4. Catalyst deposition inside microchannel.....	11
3.2.5. The selective catalyst deposition	12
3.2.6. Characterization of catalyst layer	13
3.3. Results and Discussions	13
3.4. Conclusions.....	22
3.5. Recommendations.....	23
Chapter 4. Characterization of titania layers	24
4.1. Introduction.....	24
4.2. MB Degradation experiment.....	24
4.2.1. Material preparation	24
4.2.2. Microreactor fabrication	24
4.2.3. MB Degradation experiment with microreactor.....	25
4.2.4. Simulation.....	26
4.3. Results and Discussions	27
4.4. Conclusions.....	34
4.5. Recommendations.....	35
References.....	36

Chapter 1. General Introduction

1.1. Introduction

Water is essential for living organism. Water plays a big role for mankind, from good drinking water quality to its utilization for agriculture, energy, industry, and sanitation. According to the UN [1], there are approximately 1.8 billion people in the world who still lack access to safe drinking water. Disease from contaminated drinking water and unhealthy living condition (e.g. diarrhea, cholera, dysentery and hepatitis A) can harm people's health and cause mortality. Therefore, water purification plays an important role as it provides safe water for people and other life forms. This issue is of great concern and has to be overcome by improving and developing better water treatment technologies.

In this work, we look into water treatment using photocatalysis. We investigate the degradation of methylene blue by immobilized TiO_2 catalyst in microreactor. Methylene blue (dyes) is commonly used as a model organic contaminant for water treatment research. There are some methods for dye removal such as adsorption, membrane filtration, ion exchange, electrokinetic coagulation, electrochemical destruction, etc [2]. Among these methods, photocatalysis is a promising method without any secondary pollution. Immobilized TiO_2 catalyst offers advantages that can overcome the drawback of slurry based catalyst, for instance no catalyst loss and no costly separation process due to the necessity of catalyst filtration from the aqueous phase in slurry system [3-5].

Microreactor technology has been used successfully for research in catalysis due to its large surface area to volume ratio [6]. This feature of microreactors improves heat and mass transfer [4, 6] that enhances the catalytic conversion rate. Other favourable features of microreactors are small footprint, raw materials, and minimized amount of waste. These characteristics have made microreactors more promising than other reactor types for research application.

1.2. Photocatalysis

The main reactions of photocatalysis process can be described as in Figure 1.

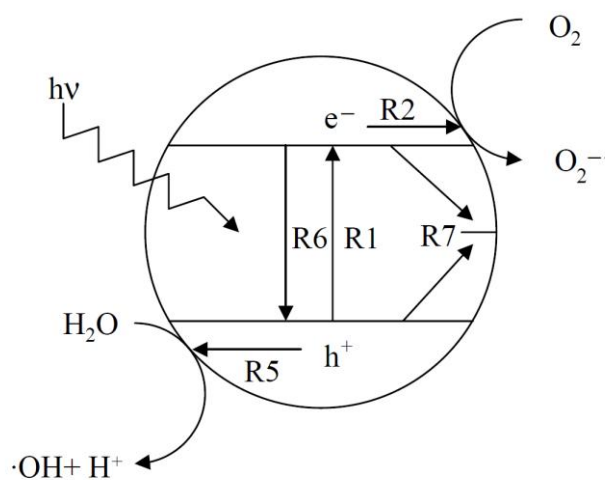


Figure 1. Reaction scheme of photocatalysis [7]

In this work, titanium dioxide or titania (TiO_2) is utilized as a photocatalyst. The initial step for heterogeneous photocatalysis is the absorption of photons [8] with energy equal to or higher than band gap energy of the semiconductor [9, 10]. The band gap energy of anatase and rutile are 3.2 eV and 3.0 eV, respectively [11]. Photoactivation of titania takes place in the range of photon wavelength of 300 - 388 nm [12].

The catalyst absorbs photons and the electrons are excited from valence band to conduction band, leaving behind positive charges (holes) in the valence band. This photoexcitation process creates charge carriers, i.e. the electrons in conduction band (CB) and holes in valence band (VB), as in Figure 1 (R1) equation (1) [11, 13, 14].



The excited e_{cb}^- reacts with oxygen molecules which are present in water to form a superoxide radical ($O_2^{\cdot-}$) as in Figure 1 (R2) equation (2) [7].



The electrons can also react with semiconductor as described in equation (3) [7].



The reaction between holes and hydroxide ions to forms hydroxyl radicals is written in equation (4) [7].



Holes also react with water which is adsorbed at the semiconductor surface [7]. This oxidative reaction creates hydroxyl radicals (OH^{\cdot}) as shown in Figure 1 (R5) equation (5) [7].



When there is no reaction between e_{cb}^- or h_{vb}^+ and other chemical species, they will eliminate each other and the energy will be lost by releasing heat. This process is known as electron-hole recombination. The direct recombination and indirect recombination are described in Figure 1 (R6 and R7), equation (6) and equation (7), respectively [7].



Dijkstra et al. [7] also mentions that for semiconductor titanium dioxide, indirect recombination will be the most likely occurrence during photocatalysis.

The generation of hydroxyl radicals is mainly governed by equation (5), but hydroxyl radicals can also be created by a sequence of radical reactions as follows [7]:





A simplified version of a reaction for hydroxyl radicals attacking organic contaminants in the adsorbed phase is described in equation (15) [15].



However, holes can also degrade the contaminant as simplified in equation (16) [15].



Photocatalysis is a technique which can be utilized to remove many dyes such as methylene blue, rhodamine B, methyl orange, and fluorescein [9].

1.3. Photocatalysts

Titanium dioxide (TiO₂), which is a well-known semiconductor photocatalyst capable of degrading organic compounds in water [3, 16, 17], is of great interest due to its low price [3, 18-21], abundant availability [22], non-toxic material [18, 23], high stability in thermal [11], chemical and biological [18, 20, 24]. TiO₂ is safe to be used in drinking water treatment process because of no formation of toxic reactive intermediate during photocatalysis reaction, and it has no taste and odour [25].

The main crystalline structures of TiO₂ are anatase (tetragonal), rutile (tetragonal) and brookite (orthorhombic) [17, 26, 27], which occur naturally at atmospheric pressures [28]. Among these main crystal structures of TiO₂, rutile and anatase are widely known for photocatalytic application [17]. One of the most used forms of TiO₂ as photocatalyst is a mixture of 70 wt% anatase and 30 wt% rutile which has high specific surface area of 72.0 m²/g [28]. Another well known commercial product is Degussa P-25 (a mixture of 80 wt% anatase and 20 wt% rutile) which has specific surface area of 49.2 m²/g [28].

The unit cell of TiO₂ are described in publication by Zhang J. et al. in literature [29] for anatase, rutile and brookite as illustrated in Figure 2.

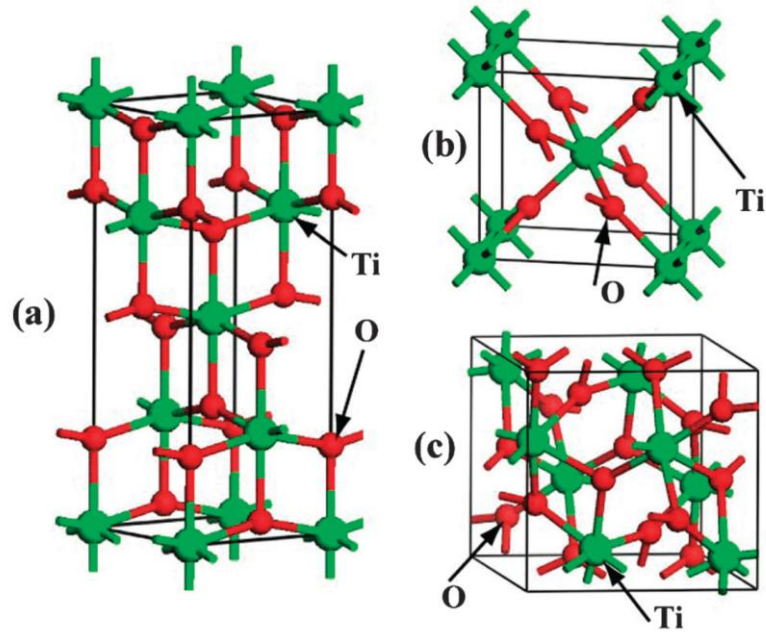


Figure 2. The crystal structure of TiO_2 (a) anatase, (b) rutile and (c) brookite [29]

1.4. Semiconductors

Pure semiconductor without doping is an intrinsic semiconductor. In the intrinsic semiconductor, the amount of electrons as negative charge carrier is equal to the amount of holes as positive charge carrier [30]. Intrinsic semiconductor can be modified to form n-type semiconductor and p-type semiconductor through doping methods for electronic application purposes [30].

In order to create n-type semiconductor, the impurities such as phosphorus, arsenic or antimony [30, 31] are added into intrinsic semiconductor. In n-type semiconductor, electrons are the major carriers and holes are the minor carriers [30]. Another characteristic of n-type semiconductor is its Fermi level (E_F) that is close to conduction band (E_C) [30], as illustrated in Figure 3.

To modify intrinsic semiconductor into p-type semiconductor, the compounds (e.g. boron, nitrogen [30], gallium or indium [31]) are used as impurities. In contrast with n-type semiconductor, p-type semiconductor has electrons as minor carriers and holes as major carriers [30], and the Fermi level (E_F) will be shifted close to valence band (E_V) [30], as illustrated in Figure 3.

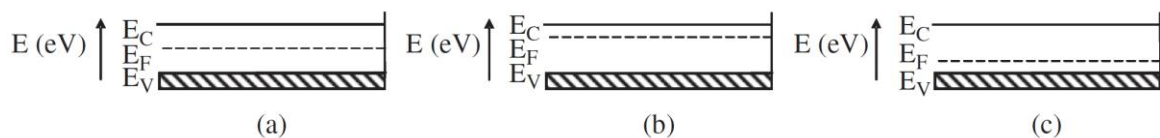


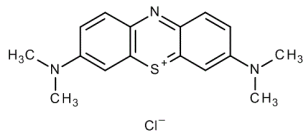
Figure 3. Energy band diagram of (a) intrinsic semiconductor, (b) n-type semiconductor and (c) p-type semiconductor [31]

1.5. Methylene blue

Methylene blue is widely used as a synthetic dye in coloring paper, dyeing textile and leather [32]. Nowadays, application of methylene blue is spreading into wider fields, for example, in biology, chemistry [10] and medicine [33]. Methylene blue is used in cardiac surgery, and its other promising uses are still undergoing research such as for vasoplegia, septic shock, hepatopulmonary syndrome and as antimalarial [33]. However, methylene blue can decrease the dissolved oxygen, which can be hazardous to water organism life [10].

Robinson [2] mentioned that there is a wide variety of dyes, which are classified into three types of dye: cationic, nonionic and anionic dyes. Anionic dyes are bright in colour, reactive in water and acid [2]. Nonionic dyes are neutral in aqueous phase [2]. Methylene blue is a cationic dye and its molecule has positive charge [34]. The properties of methylene blue are listed in Table 1.

Table 1. Chemical and Physical properties of methylene blue [35]

Name	Methylene blue
Molecular formula	$C_{16}H_{18}ClN_3S$
CAS	61-73-4
2D structure	 <p>The image shows the chemical structure of the methylene blue cation. It consists of a central benzothiazine ring system. The nitrogen atom at the top of the ring is bonded to a methyl group (CH₃). The sulfur atom at the bottom of the ring is bonded to a methyl group (CH₃) and carries a positive charge (S⁺). The two benzene rings fused to the central ring each have a dimethylamino group (-N(CH₃)₂) attached to them. Below the structure, a chloride ion (Cl⁻) is indicated as the counterion.</p>
Molecular Weight	319.851 g/mol
Color	dark green crystals
Odor	slight odor
Melting point	100 to 110 °C (with decomposition)
Solubility	43,600 mg/L at 25 °C in water
Vapor pressure	1.30×10^{-7} mmHg at 25°C
Stability	sensitive to light

Chapter 2. Scope of Research

In this research, the first part is the deposition of the catalyst layer on the microchannels. The first aim of this fabrication process is to deposit porous catalyst layers which can handle harsh operating conditions such as high temperatures and high pressures. In order to determine the adherence of catalyst layer on the substrate of microchannels, the adhesion test will be conducted. Another goal of this fabrication procedure is to utilize washcoating technique (static method and dynamic method) to pattern titania layers in various configurations. The washcoating of titania is aimed to increase surface area. Sputtering technique can be easily used for deposit TiO_2 but it leads to dense layers with low surface area. Larger surface area leads to higher conversion rates. All results will be discussed in Chapter 3. The washcoating technique proved to be unreliable and further characterization of TiO_2 was performed using dense layer fabricated by magnetron sputtering.

The second part is the characterization of titania by methylene blue degradation. In this experiment, the intrinsic surface reaction rate constant of methylene blue degradation by titania thin films is investigated using microreactor. The simulation is performed in COMSOL Multiphysics. The intrinsic surface reaction rate constant from simulation result is fitted to experimental data. By using different substrate types and pH solution, the photocatalytic performance of titania layer will be discussed. The results will be reported in Chapter 4.

Chapter 3. Fabrication of the TiO₂ catalyst layer

3.1. Introduction

There are many techniques available to deposit a thin layer of catalyst material on a substrate for instance dip coating, magnetron sputtering, atomic layer deposition, chemical vapor deposition, physical vapor deposition, sol-gel deposition, etc, that have been proposed in the literature. Hence, many of these techniques result in dense layer, whereas porous layer would increase the catalytic surface area. Unless the reaction rate is extremely fast, the availability of surface area for reaction will have a direct impact on the conversion capacity of the system. However, for most catalytic reactions, a high surface area is required. That is why, with few exceptions, dense layers like the one obtained by sputtering technique are not suitable for catalysis. In order to increase the surface area of the catalyst, the catalyst layer is deposited on the microchannel by washcoating. A good catalyst layer has good adherence to the substrate, has a uniform thickness, large surface area, and is able to withstand harsh operating condition such as high temperature and pressure.

Porous layer deposition inside microchannels is not so straightforward. Sajid Ullah et al. [36] proposed micromolding in capillaries (MIMIC), a technique to deposit the catalyst inside the microchannel which is formed by connection between substrate and mold, and uses capillary pressure as a driving force to flow the suspension inside the microchannels.

However, Huang et al. [37] and Stefanescu et al. [38] stated that the washcoating technique is the still most widely used method. D'Angelo et al. [39] proposed 2 types of washcoating technique: static and dynamic method. In the first technique, the microchannel is completely filled with TiO₂ suspension. The catalyst layer is formed on the inner walls of the microchannel by natural drying through evaporation at room temperature. In the second technique, the microchannel is filled with TiO₂ suspension, which is afterwards displaced by flushing the channel with air at different flow rate and leave TiO₂ layer on the microchannel walls. The velocity at which the suspension is displaced will define the final thickness of the catalyst layer.

D'Angelo et al. [39] stated that static method is able to achieve thicker catalyst layer, and has better uniformity and adhesion than the dynamic method. However, static method has a drawback of requiring longer time to evaporate [39]. In addition, Huang et al. [37] reported that the obstacle encountered in washcoating technique is poor catalyst adhesion due to low interaction between the substrate surface and the catalyst.

In this work, both the static and dynamic washcoating methods were evaluated as a possible deposition technique for robust catalytic layers in microfluidic channels. The purpose of this study is to fabricate and evaluate the adherence of the selective deposition of catalyst layer on the microchannel.

3.2. Catalyst deposition experiment

3.2.1. Material preparation

In this work, two types of titanium dioxide (TiO₂) suspensions were prepared. Firstly, a TiO₂ suspension of 2 wt% in methanol was made from titanium dioxide powder (TiO₂, Sigma-Aldrich, purity \geq 99.5%, size particle 21 nm). The TiO₂ powder was mixed with methanol and stirred for

24 hours at room temperature. Acetic acid was used to adjust pH value of the suspension to a value of 4-5 to prevent agglomeration of the particle in suspension [39]. Commercial TiO₂ suspensions are available in concentration of TiO₂ 30 wt% (AERODISP® VP Disp. W 2730 X) and 40 wt% (AERODISP® W 740 X). To fabricate TiO₂ suspensions at various weight percentages, the commercial 30 wt% TiO₂ was diluted in distilled water. The silicon wafers were diced into a dimension of 2 cm x 1.5 cm. To clean the surface of silicon wafer, a 1 M solution of potassium hydroxide in distilled water was prepared [39].

3.2.2. Substrate and PDMS preparation

The silicon (100) wafer was cleaned by soaking it in a 65% nitric acid solution for a minimum of 15 minutes to remove dust and contaminants. The silicon substrate was then rinsed with distilled water and dried with nitrogen gas.

A polymer base (Permacol RTV-615 A) and a curing agent (Permacol RTV-615 B) were prepared to fabricate polydimethylsiloxane (PDMS). The PDMS was prepared by cross linking of polymer base with curing agent at a mass ratio of 10 to 1. The mixture was subsequently degassed in a desiccator. The PDMS was poured into microreactor mold and degassed again in a desiccator connected to a vacuum pump. The PDMS was casted in the mold and cured at 80°C for 2 hours. The PDMS slab was then removed from the mold by cutting it. The PDMS was punctured at the two edges of the microchannel to create inlet and outlet channel.

3.2.3. Catalyst deposition on flat silicon

In the first experiments, catalyst deposition on flat silicon was conducted. PDMS with microchannels was clamped to the flat silicon wafer. The aim of these experiments was to get an idea of how to conduct the deposition, to find the bottlenecks of the washcoating technique and to characterize the titania layer.

The deposition of catalyst on the flat surface of silicon wafers was the preliminary experiment for the fabrication of patterned titania layers. In this experiment, PDMS was clamped to silicon wafers to form microchannels. PDMS is widely used in microfluidics system because it is optically transparent, cheap and non-toxic [40]. As PDMS is transparent, the suspension flows through microchannels and any leakages occurred can be directly observed.

3.2.4. Catalyst deposition inside microchannel

Two types of chips were made in silicon, differing in channel sizes: a small and a large channel. The dimension of the small channel is 250 µm in height, 250 µm in width, and 40 cm in length (Figure 4). The large channel is 250 µm in height, 500 µm in width, and 20 cm in length (Figure 5). The microchannels have UV- foil on top as a temporary cover.

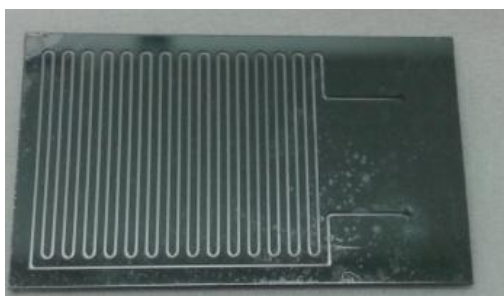


Figure 4. Microreactor with small channel (250 μm width)



Figure 5. Microreactor with large channel (500 μm width)

Firstly, KOH 1M was flushed with flow rate of $30 \mu\text{L min}^{-1}$ through the microchannel for 15 min to clean the substrate surface. Then, it was flushed with distilled water with flow rate of $30 \mu\text{L min}^{-1}$ for 15 min to removed KOH solution inside the microchannel.

The catalyst was deposited inside the microchannels by the dynamic washcoating technique. There are two chips with small microchannels. These chips were filled with 5 wt% concentration of TiO_2 . The flow rate of the suspension filling and air to displace the suspension for different chips were $10 \mu\text{L min}^{-1}$ and $30 \mu\text{L min}^{-1}$. The chip with large microchannels was filled with 5 wt% TiO_2 by using $30 \mu\text{L min}^{-1}$ flow rate for the suspension and air to displace the suspension. Subsequently, chips with catalyst layer on the microchannel walls were calcined at $300 \text{ }^\circ\text{C}$ for 8 h at a heating rate of $2 \text{ }^\circ\text{C min}^{-1}$ and a cooling rate of $2 \text{ }^\circ\text{C min}^{-1}$.

3.2.5. The selective catalyst deposition

In the next step, the catalyst was deposited in various patterns. The microchannel that was used to deposit patterned titania layer is illustrated in Figure 6. The microchannels were made in silicon with a width of $600 \mu\text{m}$, a height of $50 \mu\text{m}$, and a length of 6 cm. The PDMS has protruding slabs, so when it is attached to the silicon, it makes a pattern of small channels inside a big channel as described in Figure 6 (b). In this work, PDMS have two types of patterns: 3 small $100 \mu\text{m}$ width channels and 5 small $60 \mu\text{m}$ width channels that are parallel to the silicon channel. The PDMS with 3 small channels pattern has 3 protruding slabs of the same height as the silicon channel and dampen part in sequence. The distance between the slabs that makes up the new microchannel has the same width as the protruding slab.

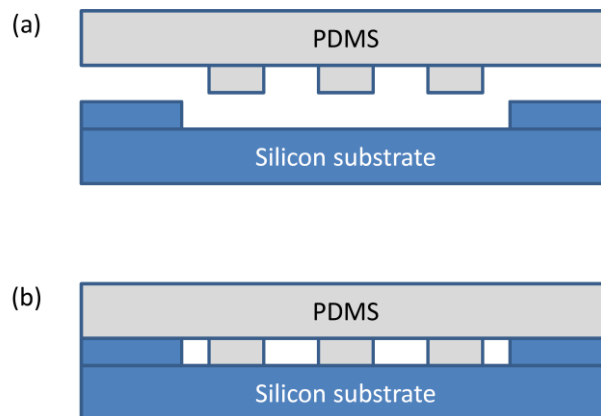


Figure 6. Microchannel for selective titania deposition

3.2.6. Characterization of catalyst layer

The morphology of catalyst layer was analyzed with scanning electron microscope (SEM). The thickness and the homogeneity of catalyst layer were also observed by SEM analysis. The adhesion test of the catalyst layer to the microchannel was performed by heating the coated microchannels in boiling water at a temperature of 100°C for 1 hour. The catalyst layer before and after adhesion test was visualized by SEM.

3.3. Results and Discussions

The unsuccessful catalyst layer deposition on the flat silicon surface was caused by leakage. Figure 7 shows a white pattern which is suspensions that overflows from the microchannels and covers the part of substrate surface. During the experiment, leakage occurred at the inlet and outlet of the microchannels and along the microchannels. This leakage problem is likely to occur due to poor adhesion of PDMS to the silicon substrate. The PDMS was slightly lifted up from the silicon substrate, which may occur if the PDMS cannot hold the applied pressure when suspension is being injected. Another reason may be deformation of PDMS that is caused by inserted needles to create inlet-outlet channel, where it can make the PDMS to become slightly bended at the inlet-outlet area when PDMS is clamped to substrate.

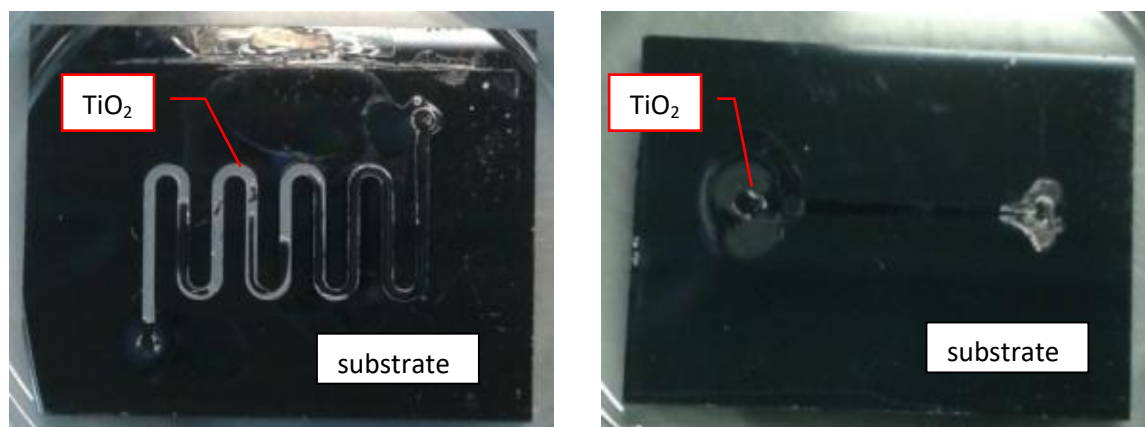


Figure 7. Pictures of leakage in titania deposition obtained with 30 wt% TiO_2 suspension by using static method (left side) and dynamic method (right side)

In order to overcome leakage problem, some attempts had been done. To reduce the leakage problem at the inlet and outlet, flexible tubing were used instead of needles, which aimed to reduce the deformation of the PDMS. However, this attempt was unsuccessful because the PDMS was still lifted up when it was clamped to silicon substrate.

In addition, instead of clamping the PDMS to the silicon, the temporary bond of PDMS and the silicon substrate needed to be improved. The silicon was treated by oxygen plasma to remove any contaminants before it was attached to the PDMS, however; it did not solve the leakage problem either.

Lastly, partial curing of the PDMS was tried to solve the leaking, as it should improve the adhesion of PDMS to silicon. Usually, PDMS is cured at 80°C for 2 hours [40], which is required for complete cross-linking of the polymer base with addition of curing agent. The operating parameter of partial curing of the PDMS that were conducted in this experiment is listed in Table 2. At first curing, the PDMS with partial curing method from Hoon was cured at certain time and temperature. Then the PDMS was cut and attached to silicon substrate. The silicon substrate with PDMS on top was cured again to obtain complete curing of PDMS. However, none of these operating conditions of partial curing method can solve leakage problem.

Table 2. The parameter of partial curing of the PDMS

Partial curing PDMS	First curing		Last curing	
	Temperature	Time	Temperature	Time
Batch 1	80°C	45 min	80°C	overnight
Batch 2	70°C	40 min	70°C	overnight
Batch 3	80°C	45 min	80°C	1.5 hours

The leakage of washcoated catalyst layer obtained by dynamic technique using 40 wt% TiO₂ is shown in Figure 8 (left side). In addition, incomplete wetting of the silicon surface by the suspension was observed as seen in Figure 8 (right side). Dewetting of the suspension on the surface of silicon may be caused by the contamination of the silicon surface by organic compounds from PDMS when the silicon was attached to PDMS during heating to reach complete cross linking in the procedure of PDMS with partial curing.

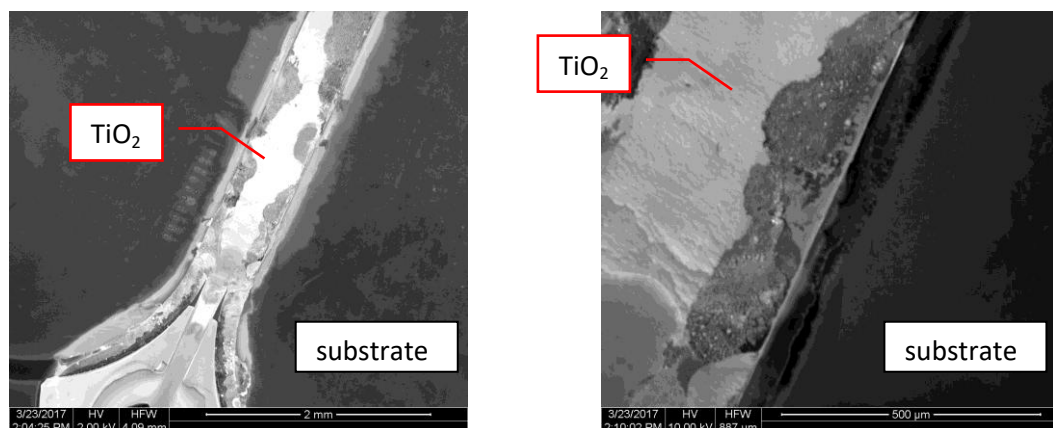


Figure 8. SEM images of titania washcoat obtained by using dynamic method at flow rate $30 \mu\text{L min}^{-1}$ with suspension 40 wt% TiO_2 showing leakage (left side) and dewetting (right side)

The morphology of washcoated catalyst layer obtained by static technique using different TiO_2 concentration i.e. 2 wt% TiO_2 in methanol and 30 wt% TiO_2 from commercial suspensions can be observed in Figure 9. Higher TiO_2 concentration in the suspension results in a thicker catalyst layer. However, we cannot use these data to determine effect of TiO_2 concentration on the thickness of catalyst layer because of above mentioned leakage problem that probably influences the uniformity of catalyst loading into microchannels and the drying process of catalyst layer. In other words, the suspension is evaporating faster at the point of leaking.

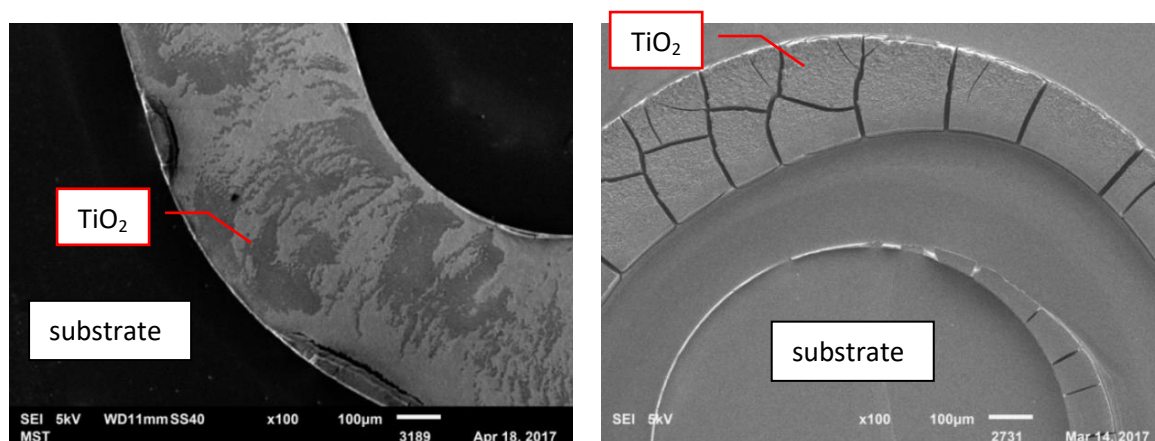
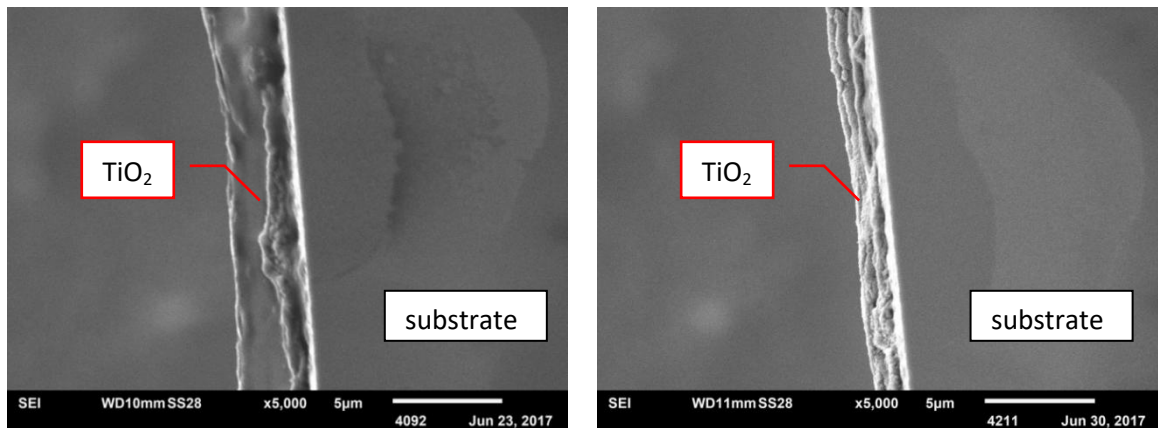


Figure 9. SEM images of titania washcoat obtained by using static method. Left side: with 2 wt% TiO_2 in methanol. Right side: with commercial suspensions 30 wt% TiO_2

In the next part, to investigate the feasibility of selective catalyst coating inside microchannels, dynamic washcoating method was applied to the microreactor with UV-foil as a temporary lid. This method uses suspension 5 wt% TiO_2 with various flow rates of air ($10 \mu\text{L min}^{-1}$ and $30 \mu\text{L min}^{-1}$) to displace the catalyst suspension leaving titania layers in the small channels.

Figure 10 shows that the thickness of catalyst layer in the small channels obtained by using dynamic method decreases after calcination. As the concentration of TiO_2 is low (5 wt%), the water content that evaporates during the calcination is high. SEM image after calcination shows that the catalyst layer is noticeably uniform without visible crack and adheres to the substrate.

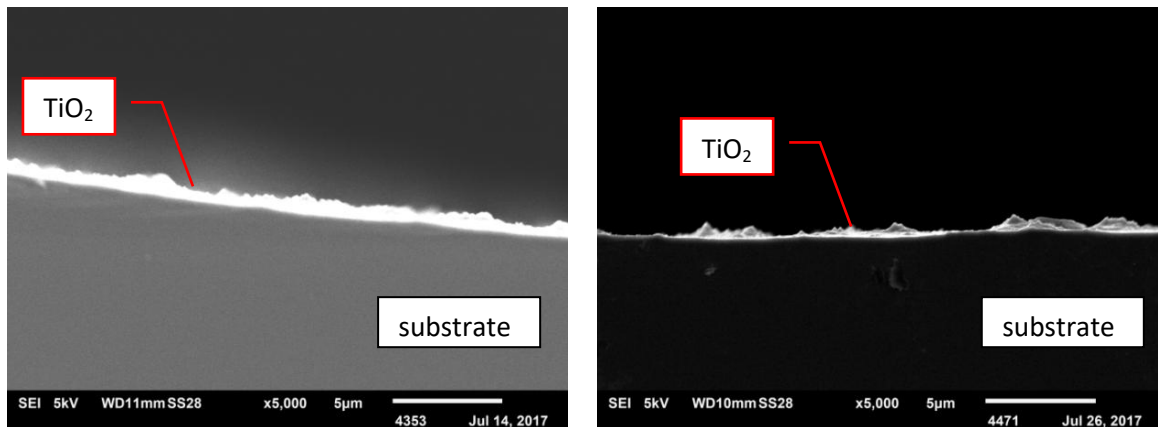


(a) before calcination

(b) after calcination

Figure 10. SEM images of titania washcoat on the outside of L bend of small channels obtained by using dynamic method at flow rate $10 \mu\text{L min}^{-1}$

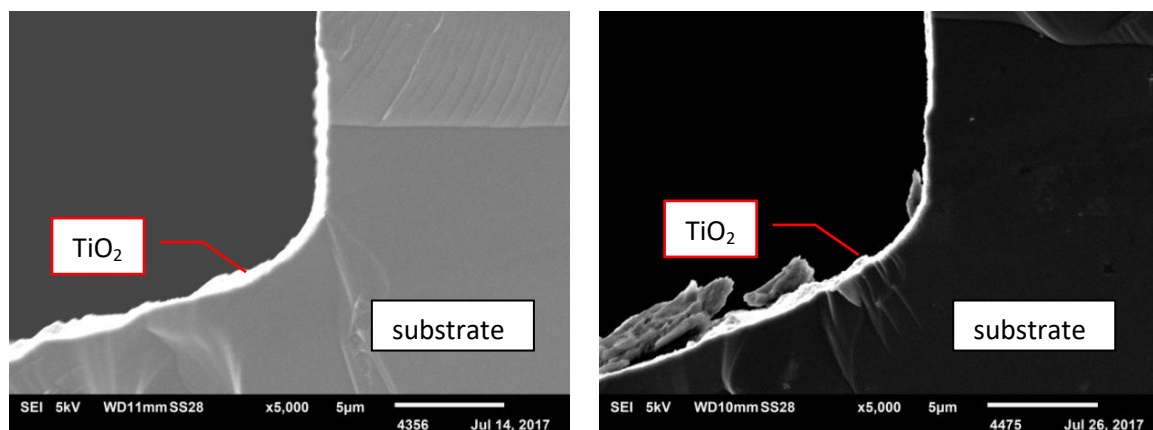
Figure 11 and Figure 12 show the cross section view of catalyst layer in the bottom small channel that was obtained by using dynamic technique at flow rate $10 \mu\text{L min}^{-1}$ with suspension 5 wt% TiO_2 for the suspension filling and displacement. Although, it is difficult to reproduce SEM images at the same spot with the same focus plane, we assume there would be no significant visible distinction between before and after adhesion test.



(a) before adhesion test

(b) after adhesion test

Figure 11. Cross sectional SEM images of titania washcoat on the bottom of small channels obtained by using dynamic method at flow rate of $10 \mu\text{L min}^{-1}$

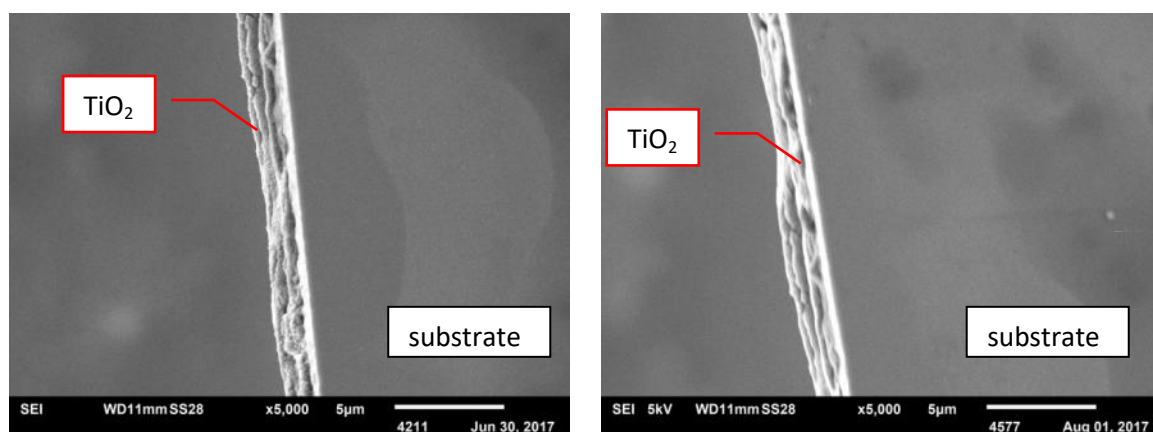


(a) before adhesion test

(b) after adhesion test

Figure 12. Cross sectional SEM images of titania washcoat on the bottom corner of small channels obtained by using dynamic method at flow rate $10 \mu\text{L min}^{-1}$

Figure 13 shows the catalyst layer that was obtained by using dynamic method at flow rate $10 \mu\text{L min}^{-1}$ for the suspension filling and displacement at the U bend in small channel from top view. Again as in previous SEM images, the SEM image in Figure 13 shows the catalyst layer remains unchanged after adhesion test.



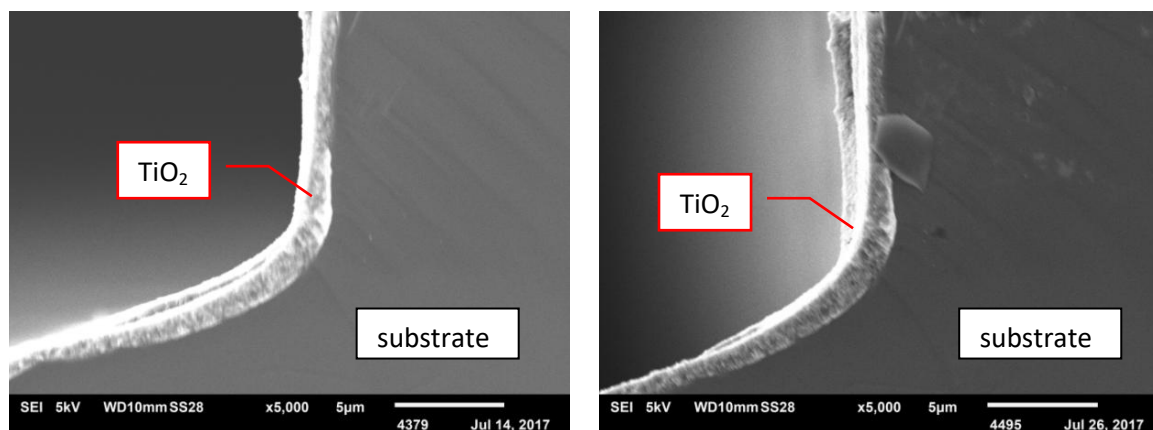
(a) before adhesion test

(b) after adhesion test

Figure 13. SEM images of titania washcoat on the outside of the U bend of small channels obtained by using dynamic method at flow rate $10 \mu\text{L min}^{-1}$

Next, the deposition of catalyst layer onto small channel by using dynamic method with suspension 5wt% TiO_2 at flow rate $30 \mu\text{L min}^{-1}$. The different flow rate of air flushing from previous small channel was applied to investigate the effect of various speeds of suspension displacement on catalyst layer thickness.

Figure 14 shows the SEM image at cross section of catalyst layer at the bottom corner of small channels.

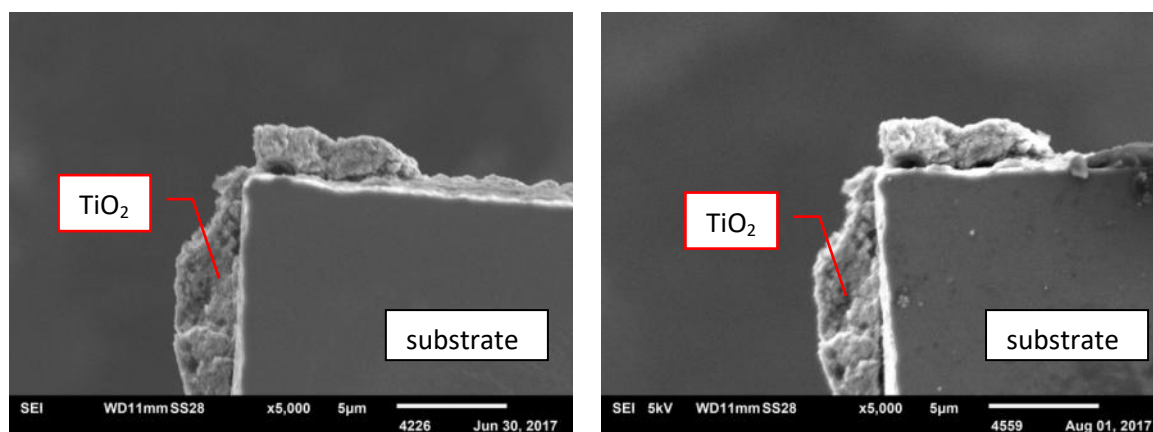


(a) before adhesion test

(b) after adhesion test

Figure 14. Cross sectional SEM images of titania washcoat on the bottom corner of small channels obtained by using dynamic method at flow rate $30 \mu\text{L min}^{-1}$

Figure 15 shows the catalyst layer which was obtained at the sharp turn (at L bend channel) from the top view, indicating an accumulation of catalyst in the sharp turn. The SEM image after adhesion test shows that there are some particles scattered on the substrate that might come from the catalyst layer.



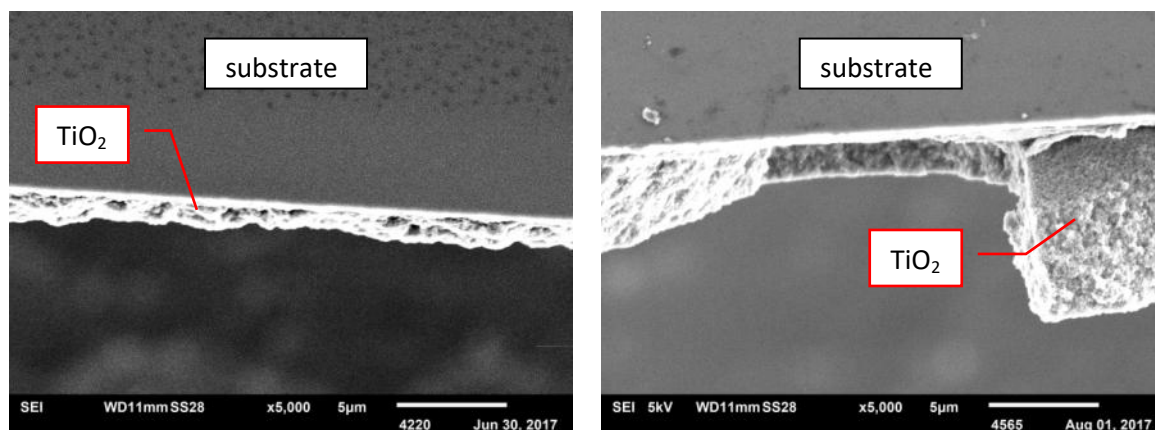
(a) before adhesion test

(b) after adhesion test

Figure 15. SEM images of titania washcoat on the inside of the L bend of small channels obtained by using dynamic method at flow rate $30 \mu\text{L min}^{-1}$

Figure 14 and Figure 15 show the good adherence of titania layer to the substrate for catalyst layer in small channel that was obtained by using dynamic technique with $30 \mu\text{L min}^{-1}$ flow rate. There is no obvious difference between the catalyst layers at before and after adhesion test.

Figure 16 (b) shows different thickness of the catalyst layer at different locations. The observed thick catalyst layer may come from the catalyst that was stuck on the UV foil. Therefore, SEM analysis at cross section of microchannels is required to determine the catalyst layer thickness.

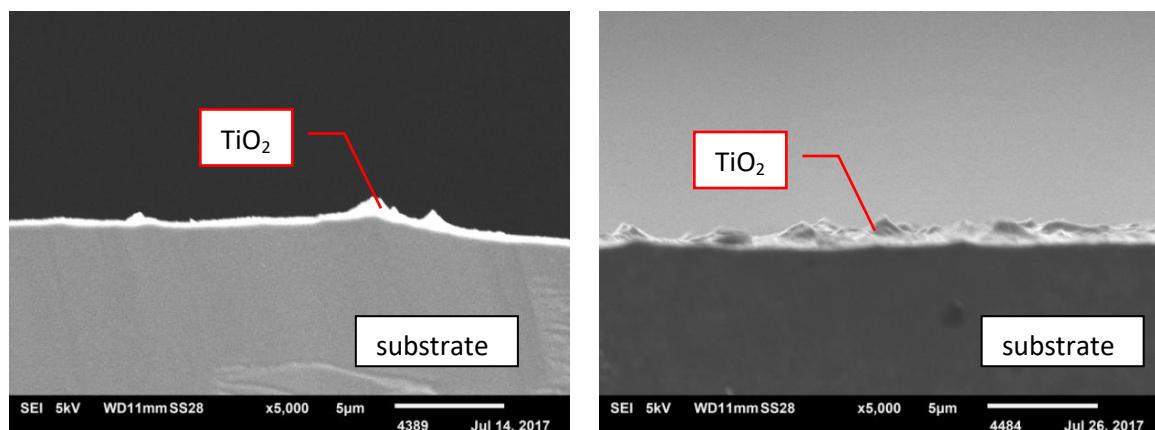


(a) before adhesion test

(b) after adhesion test

Figure 16. SEM images of titania washcoat on the straight channel of small channels obtained with by using dynamic method at flow rate $30 \mu\text{L min}^{-1}$

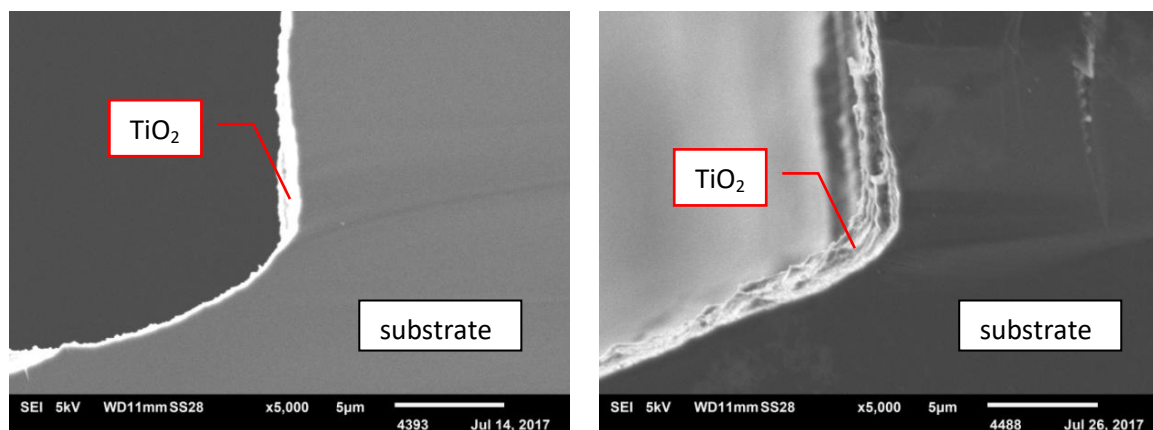
In the next step, fabrication of catalyst layer was also conducted on microreactors with large channels where its width is twice the width of microreactor with small channels. Figure 17, Figure 18 and Figure 19, indicate that the catalyst layer still adheres to the microchannel walls. Comparison between SEM images before and after adhesion test could not be done straightforwardly because it was difficult to reproduce SEM image at the same spot with the same focus plane on the substrate.



(a) before adhesion test

(b) after adhesion test

Figure 17. Cross sectional SEM images of titania washcoat on the bottom of large channels obtained by using dynamic method at flow rate $30 \mu\text{L min}^{-1}$



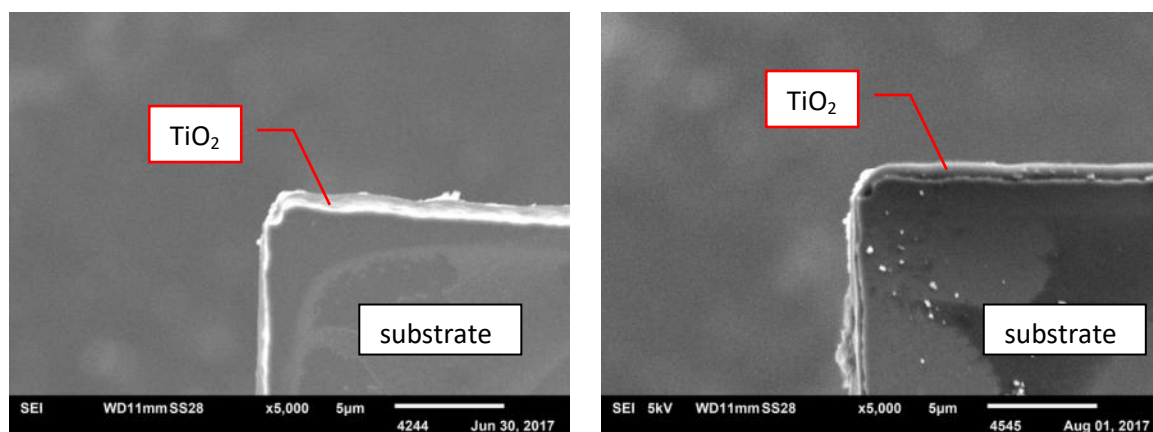
(a) before adhesion test

(b) after adhesion test

Figure 18. Cross sectional SEM images of titania washcoat on the bottom corner of large channels obtained by using dynamic method at flow rate $30 \mu\text{L min}^{-1}$

Again, as can be seen in Figure 18, the comparison of SEM images between before and after adhesion test is not conclusive because of the difficulty in reproducing the same focus plane.

Figure 19 shows that after the adhesion test there are some particles scattered on the substrate surface that might be from catalyst loss. However, there is no noticeable damage occurs on the catalyst layer. Therefore, we can conclude that the catalyst loss after adhesion test is minimal.



(a) before adhesion test

(b) after adhesion test

Figure 19. SEM images of titania washcoat on the inside of the L bend of large channels obtained by using dynamic method at flow rate $30 \mu\text{L min}^{-1}$

We found that the determination of catalyst thickness in this work is difficult because it requires a high resolution SEM image of cross section view. In this result, the quality of the high magnification image is low and the catalyst layer is difficult to be found on the substrate. In order to observe the catalyst layer, high resolution SEM would be required. A better cutting procedure for the chips is also necessary because as noticed in the SEM cross section view the catalyst layer was sometimes peeled off. However, we tried to estimate the catalyst thickness at the bottom corner of the channels from SEM images although the result is not exact number. The rough estimation of catalyst layer thickness from SEM images of catalyst layer on the

bottom corner of microchannels obtained by using dynamic method with suspension 5 wt% TiO₂ for different geometry channel and flow rate is listed in Table 3.

Table 3. The rough estimation of catalyst layer thickness on the bottom corner of channels obtained by using dynamic method

Parameter	Catalyst layer thickness, μm
small channels with 5 wt% TiO ₂ , flow rate 10 $\mu\text{L min}^{-1}$	0.5 - 1.0
small channels with 5 wt% TiO ₂ , flow rate 30 $\mu\text{L min}^{-1}$	2.0 - 2.5
big channels with 5 wt% TiO ₂ , flow rate 30 $\mu\text{L min}^{-1}$	0.5 - 1.0

The catalyst thickness of two different suspension displacement flow rate (10 $\mu\text{L min}^{-1}$ and 30 $\mu\text{L min}^{-1}$) for small channels chips shows higher speed displacement give result in thicker catalyst layer. Theoretically, increasing the suspension displacement velocity increases the thickness of catalyst layer. According to Taylor [41] who was referring to the experiment of Fairbrother & Stubbs, the fraction of the catalyst layer in a capillary tube obtained from displacing suspension by flushing air can be calculated from equation (17).

$$m = \left(\frac{\mu \times v}{\sigma} \right)^{\frac{1}{2}} \quad (17)$$

Where m is fraction of catalyst layer, μ is the suspension viscosity, v is the speed of suspension displacement, and σ is the suspension surface tension [39].

Unfortunately, we did not measure the properties of suspension 5 wt% TiO₂ that we used, such as surface tension and viscosity. However, we tried to do approximation by using equation (17) for water with the same parameter in this experiment such as geometry of microchannel and flow rate to displace the suspension. The velocity of suspension displacement can be calculated from the flow rate and cross section of area in the microchannel. The fraction of catalyst layer (m), we described as the ratio of weight per unit length [41] of suspension that left inside the microchannel to initial weight per unit length of suspension filled the microchannel. Hence, the rough calculation of water layer thickness that left after flushing with air inside the small channel at flow rate 10 $\mu\text{L min}^{-1}$ is 0.38 μm and 0.65 μm for flow rate 30 $\mu\text{L min}^{-1}$; and big channel at flow rate 30 $\mu\text{L min}^{-1}$ is 0.46 μm . Although, these numbers are not come from calculation with catalyst suspension properties, we can assume the above equation can be used to explain that catalyst layer thickness corresponds to suspension displacement velocity and it is possible to use equation (17) to predict the catalyst thickness.

Table 3 shows that the big channel produces thinner catalyst layer than small channel with the same flow rate. As the width of big channel is twice of the small channel, the velocity of air in the big channel to displace the suspension is a half of that in small channel. As above mentioned, the small displacement speed occurs in big channel results in thinner catalyst layer despite the same value of air flow rate used to displace the suspension. In other word, the catalyst thickness is defined by the speed of suspension displacement (m s^{-1}).

From the SEM image, the homogeneity of catalyst layers is quite uniform although in some sharp bends layers with different thickness were also observed.

The observation of catalyst layer after adhesion test is difficult because it requires to reproduce the SEM image at the same spot with the same focus plane. As mentioned before, high resolution SEM and better cutting procedure for the chips are immensely required to observe the adherence of catalyst layer on the substrate.

The last part of this fabrication procedure is deposition of patterned titania layer in various configurations by using static method. Figure 20 and Figure 21 show the patterned titania layer by using 3 channels and 5 channels of PDMS, respectively. These figures show that leakage occurs at the inlet - outlet and along the microchannels.



Figure 20. Patterned titania with 3 channels obtained with 30 wt% TiO₂ by using static method



Figure 21. Patterned titania with 5 channels obtained with 30 wt% TiO₂ by using static method

As mentioned in the part of the catalyst deposition on the flat silicon surface, the leakage is likely to occur due to the poor adhesion of PDMS to the silicon substrate. The deformation of PDMS also caused leakage at inlet-outlet. When inlet-outlet tubing was inserted into the PDMS, it made the PDMS bend slightly and it caused leakage at the inlet and outlet area. In addition, the PDMS could not hold the applied pressure of suspension when it was being injected through the microchannel and caused leakage along the channel. Using of PDMS as temporary lid for catalyst deposition may not be such a good idea because some TiO₂ suspension stuck on PDMS. When PDMS was lifted from the substrate, some catalyst layer was also removed together with PDMS. As we can see in Figure 20 and Figure 21, the patterned catalyst layers were fragmented after the PDMS was peeled off from microchannels.

3.4. Conclusions

The fabrication of patterned catalyst layers on microchannels has some obstacles such as leakage problem due to poor adhesion between PDMS and the substrate, and the adherence of the suspension on PDMS may damage the catalyst layer when PDMS is removed from the substrate.

The observation of the adherence of the catalyst layer to the microchannel in some spot on the substrate show good results. However, a little amount of catalyst particles was found scattered on the surface of substrate. In other word, we could conclude that the loss of catalyst after adhesion test is minimal.

The catalyst layer thickness could not be properly determined due to the low resolution of the SEM images and the cutting process of chip that might have destroyed the catalyst layer. However, rough estimation from SEM images of catalyst thickness shows that increase in suspension displacement speed (m s^{-1}) increases the thickness of catalyst layer.

3.5. Recommendations

In order to investigate the catalyst layer deposition on the microchannel, the SEM analysis is conducted. The SEM analysis is a crucial characterization technique to characterize the morphology of catalyst layer, to determine catalyst layer thickness and observe the adherence of catalyst layer to microchannel.

Therefore, it is highly recommended to use high resolution SEM. In addition, better cutting procedure for the chip is required in the preparation of samples for SEM analysis to give accurate observation on the cross section view. In this work, the cutting protocol for the chip is at first dicing the chip from the backside until the half of chip thickness. Then break the chip thoroughly. For future experiment, we recommend to cut the chip thoroughly to get clear cut cross section.

In order to evaluate the thickness of catalyst layer from experimental results, suspension properties such as viscosity and surface tension can be evaluated as a starting point.

Chapter 4. Characterization of titania layers

4.1. Introduction

Photocatalysis using titania is a part of AOP (Advanced Oxidation Process) which generates hydroxyl radicals (OH^*) during the process. Photocatalysis is a promising technology that can be utilized to degrade both organic and inorganic contaminants in water treatment [42]. The frailty of photocatalysis is hydroxyl radicals having short half-life in order of microseconds which is not suitable to destroy pathogens for disinfection purposes [42].

However, photocatalysis using titania has the advantages that no secondary pollution is produced [7], its by-products are usually CO_2 and H_2O , and it requires mild operation [21]. Moreover, there are no additional chemicals involved in the photocatalysis process [43]. These advantages have promoted photocatalysis as an attractive technology for water treatment research.

In this work, the characterization of titania by MB degradation is conducted. The photocatalysis degradation of MB by titania in microreactor was investigated by determining the intrinsic surface reaction rate constant from experimental data and modeling with COMSOL Multiphysics. The MB degradation by titania layer on various of substrates, pH solution are discussed in this chapter.

4.2. MB Degradation experiment

4.2.1. Material preparation

In this work, three substrate types, i.e. silicon dioxide (SiO_2), p-type silicon (p-Si) and n-type silicon (n-Si) onto which TiO_2 thin films are coated. These thin dense films were prepared by sputtering technique. The substrate (p-Si, n-Si and SiO_2) with 200 nm TiO_2 coating on top with a dimension of 2 cm x 1.5 cm was cleaned by soaking in nitric acid solution 65% for a minimum of 15 minutes to remove dust and contaminant. Then silicon substrate was rinsed with distillate water and dried with nitrogen gas.

Methylene blue (MB) solution with a concentration of 40 μM was prepared by diluting 1 mM MB solution with distilled water. The pH of MB solutions were determined by pH meter. MB solutions with a concentration of 40 μM were prepared for three pH solution values: pH 3, 6 and 9 by adding small quantity of hydrochloric acid (HCl) or sodium hydroxide (NaOH).

4.2.2. Microreactor fabrication

PDMS microchannel fabrication was described in section 3.2.2. The microreactor was made of PDMS microchannel and TiO_2 thin film on the substrates as photocatalysts. The fabrication of microreactor is illustrated in Figure 22. The microchannel has a dimension of 50 μm height, 500 μm width and 5.96 cm length. The total volume of the microreactor is approximately 1.49 μL .

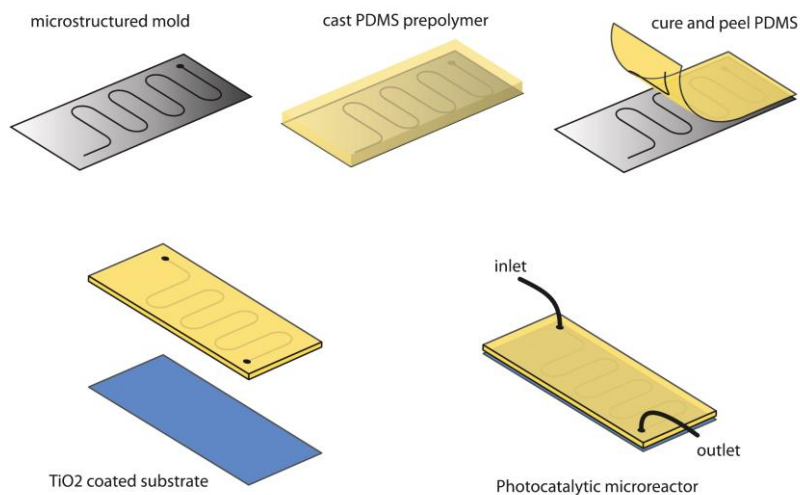


Figure 22. Fabrication of photocatalytic microreactor [44]

4.2.3. MB Degradation experiment with microreactor

The experimental setup of MB degradation is illustrated in Figure 23. MB solution with a concentration of $40 \mu\text{M}$ was pumped into the microreactor with flow rates of 5, 10, 15, 30 and $50 \mu\text{L min}^{-1}$ for each variant pH solution and substrate types. The UV-Vis spectrometer Ocean Optics was used to observe the absorbance of MB at a wavelength of 664.10 nm. The experiment for degradation of MB was conducted by using UV light source at 100% power at a distance of 14 cm from the surface of microreactor. The light source used LEDs which emits UV light at 365 nm wavelength. This setting gave 80 mW cm^{-2} photon flux density. The temperature of the microreactor was set at 20°C .

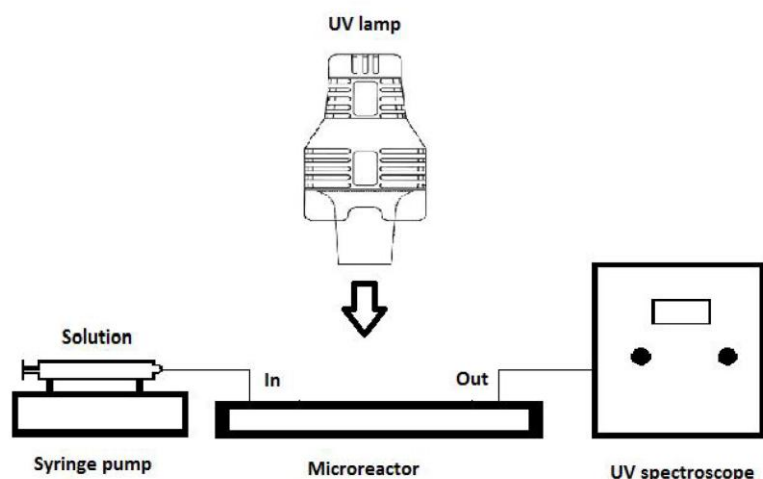


Figure 23. MB degradation experiment setup [44]

4.2.4. Simulation

The results from the MB degradation using microreactors with continuous catalyst layer were used to fit the intrinsic surface reaction rate constant. A model was established to describe the convection, diffusion and reaction rate. The model was solved in COMSOL Multiphysics. The intrinsic surface reaction rate constant was determined by fitting the numerical results to the experimental data. The model of the microchannel in 2D is illustrated in Figure 24.

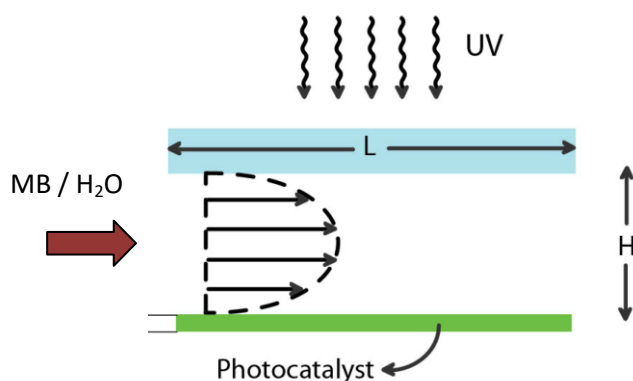


Figure 24. Model of the microchannel in 2D [44]

In this model, mass balance in the flow channel is governed by convection and diffusion with the reaction rate as flux boundary conditions.

Many authors [3, 4, 20, 21, 45] proposed Langmuir-Hinshelwood (L-H) rate expression to describe photocatalytic reaction on the catalyst surface, which is written in equation (18) [9].

$$R = k \left(\frac{KC}{1+KC} \right) \quad (18)$$

Where k is intrinsic reaction rate constant, K is the adsorption constant of reactant in dark environment and C is the concentration of reactant [9].

However, Hermann [9] stated that for diluted solution where concentration of the reactant is less than 1×10^{-3} M, KC value becomes very small and the reaction can be simplified as first order reaction. In this work, we assume the reaction rate of MB consumption is a first order reaction due to the initial concentration of MB is 40×10^{-6} M.

The reaction rate is assumed as first order reaction with respect to MB as in equation (19).

$$R = k'' c \quad (19)$$

In this equation, R is reaction rate with unit in $\text{moles m}^2 \text{ s}^{-1}$, k'' is the intrinsic surface reaction rate constant with unit in m s^{-1} and c is concentration of MB with unit in moles m^{-3} .

We assumed that convection occurs in x direction and diffusion occurs in y direction. The mass balance which includes the convection and diffusion terms is written in equation (20).

$$u(y) \frac{\partial c}{\partial x} = D \frac{\partial^2 c}{\partial y^2} \quad (20)$$

In this equation, $u(y)$ is the fluid velocity, c is the reactant (MB) concentration, and D is the diffusion coefficient for MB in water. According to Rafieian et al. [46], the molar diffusion coefficient for MB in water is $5.7 \times 10^{-10} \text{ m}^2\text{s}^{-1}$.

The parabolic velocity profile in the flow channel is determined by solving Navier-Stokes equation in two dimensions for the Cartesian system, and it is assumed that the flow between two parallel flat plates is steady state and laminar.

Hence the parabolic velocity profile is given by equation (21).

$$u(y) = u_{avg} \left(\frac{-6y^2}{H^2} + \frac{6y}{H} \right) \quad (21)$$

The boundary condition at the upper wall is zero flux, which means there is no flux through the upper wall.

at $y = H$

$$D \frac{\partial c}{\partial y} = 0 \quad (22)$$

The bottom boundary condition, at the catalyst surface, is the flux equal to the consumption rate of MB.

at $y = 0$

$$D \frac{\partial c}{\partial y} = k'' c \quad (23)$$

4.3. Results and Discussions

In this work, the influence of pH solution on the degradation of MB by titania thin film coated on n-type silicon (n-Si), p-type silicon (p-Si) and silicon dioxide (SiO_2) substrates are presented.

Three solutions of different pH were chosen as representatives of acidic solution (pH 3), neutral solution (pH 6) and basic solution (pH 9). It is important to consider the pH of solutions because the surface charge of semiconductor is affected by pH [11, 30], which has implications on the photocatalytic activity. Point of zero charge (Pzc) is the pH at which the surface charge of materials is neutral [47]. The Pzc of TiO_2 thin film which is fabricated on p-type Si (100) wafers (8–12 Ω cm) is achieved at pH 6.2 [47]. Other references reported that Pzc of TiO_2 is 5.8 [30], 6.25 [48], while Pzc for Degussa P25 is 6.4 [49]. According to references [11, 48, 50], the surface charge of TiO_2 under pH condition lower than Pzc and pH condition higher than Pzc follows equations (24) and (25), respectively.



The result of the MB degradation by titania thin films coated on the n-Si, p-Si and SiO_2 substrates at three different values of pH solutions are shown in Figure 25, Figure 26 and Figure 27.

The degradation of MB was calculated as in equation (26) [46].

$$\text{Degradation} = \frac{C_o - C_f}{C_o} \times 100\% \quad (26)$$

Where C_o is the initial concentration of MB and C_f is the final concentration of MB. The initial and final concentrations of MB were determined by quantifying the absorbance of MB for the microreactor output stream by using UV-Vis spectrometer.

The lines in Figure 25, Figure 26, and Figure 27 represent the results from simulation, which were adjusted to fit experimental data indicated by the data points in the graph. The determination of intrinsic surface reaction rate constants (k'') were performed in COMSOL Multiphysics, taking into account mass transfer by convection and diffusion. The fitted intrinsic surface reaction rate constants for various substrates at various pH of the solutions are listed in Table 4.

Table 4. Intrinsic surface reaction rate constant (unit in m s^{-1}) of photocatalytic degradation of MB by titania

pH	n-type silicon substrate	p-type silicon substrate	silicon dioxide substrate
3	2.5×10^{-6}	1.1×10^{-6}	1.5×10^{-6}
6	8.8×10^{-6}	5.9×10^{-6}	8.6×10^{-6}
9	1.1×10^{-5}	9.8×10^{-6}	9.6×10^{-6}

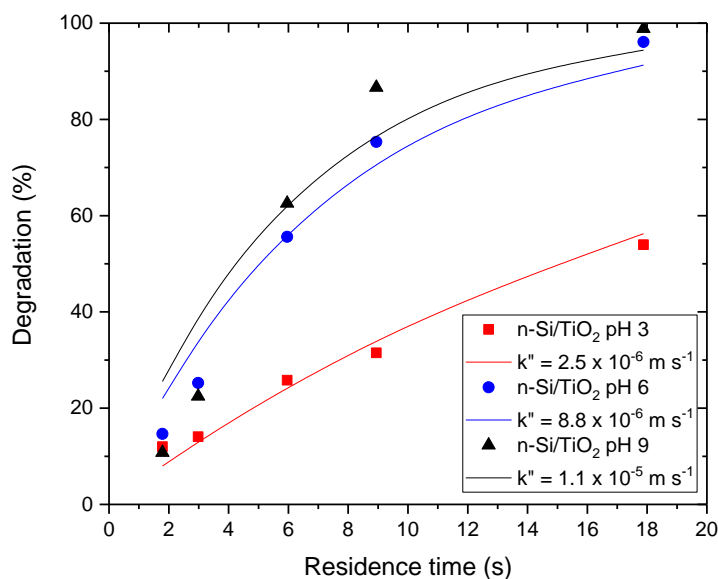


Figure 25. The degradation of MB by titania on n-Si substrate

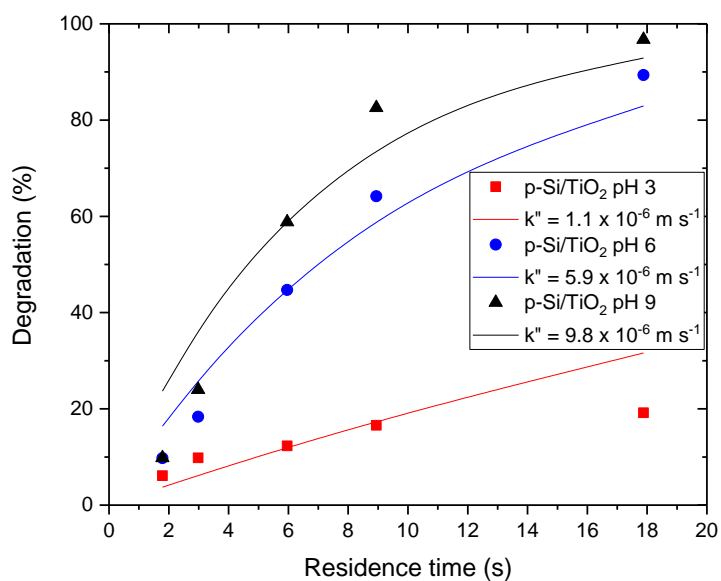


Figure 26. The degradation of MB by titania on p-Si substrate

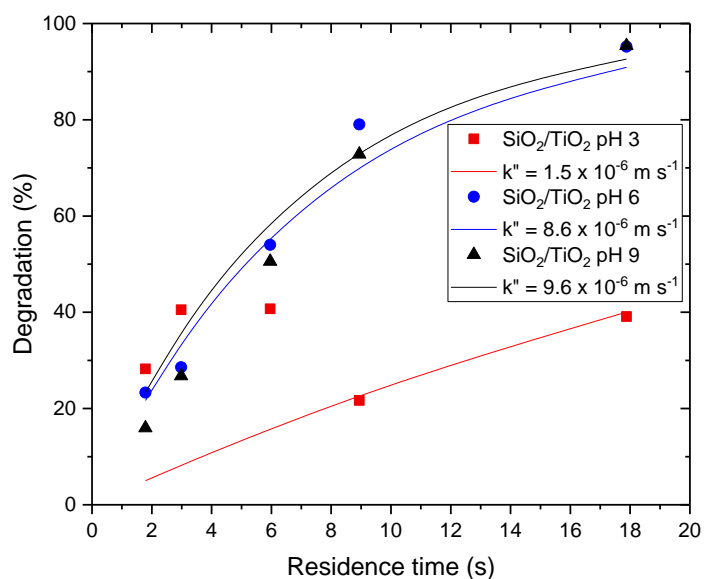


Figure 27. The degradation of MB by titania on SiO₂ substrate

The error in the measurement probably come from the uncertainty of UV-Vis spectrophotometer, such as the presence of bubbles in the system and the MB adsorption on the windows of the flow cell of UV-Vis spectrometer, which can reduce the accuracy of the absorbance reading of UV-Vis spectrometer. Moreover, during measurement, the PDMS of the

microreactor adsorbs MB, which can result in a reduction of intensity of the UV-light penetrating the microreactor. Another source of deviation may emerge from a small gradient in the temperature. A Peltier element was used to control the temperature of microreactor at 20°C which usually took some time to achieve a stable temperature value. Observation during experiment has shown that the UV-Vis spectrometry recorded high absorbance of MB with increasing temperature. The temperature influences the adsorption of MB to the catalyst surface which decreases with increasing temperature.

The degradation of MB for three variations of substrates (n-Si, p-Si and SiO₂) increases with higher residence time. High residence time leads to longer contact time between MB and the catalyst in the microreactor and increase the conversion rate.

Many authors [12, 19, 30, 51, 52] reported that the adsorption of compounds to TiO₂ due to the different surface charge of TiO₂ at the corresponding pH. At acidic solution, i.e. pH 3, where pH is lower than Pzc, the concentration of protons (H^+) of the bulk phase increases [12], and the surface charge of TiO₂ become positively charged by adsorbing protons (H^+) following equation (24). There is a strong repulsion between the positively charged catalyst surface and cationic dye (MB) molecules. This strong repulsion leads to decreasing adsorption of MB dye on the catalyst surface. When the adsorption of MB of the catalyst surface is hindered, hence the photocatalytic degradation of MB decreases.

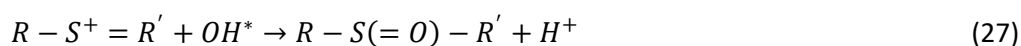
The surface charge of TiO₂ at pH 6 is in the neutral range as pH solution of 6 is close to Pzc of TiO₂. This neutral surface charge leads to no repulsion and attraction towards the MB molecules. Therefore, the photocatalytic degradation of MB at pH 6 is in the range between pH 3 and pH 9 because the adsorption of MB molecules to catalyst surface is not as low as at pH 3 or as high as at pH 9.

At pH 9, which is higher than Pzc of TiO₂, concentration of hydroxide ions (OH^-) increases [51] and the surface charge of TiO₂ becomes negatively charged by adsorbing hydroxide ions following equation (25). As the surface of catalyst is negatively charged, strong attraction towards the cationic compounds occurs and enhances the adsorption of cationic compounds on the catalyst surface, which results in increasing MB degradation.

Moreover, according to Ahmed et al. [19], at pH 9 there is excess of hydroxide ions (OH^-) which facilitate the formation of hydroxyl radicals (OH^*) by reaction with holes (h_{vb}^+) following equation (4) which was mentioned in chapter 1.



The surplus of hydroxyl radicals increases the photocatalytic activity of the catalyst because the hydroxyl radicals can directly attack the bond of the $C-S^+=C$ of MB, which is described in equation (27) [51].



Theoretically, the degradation of MB increases with higher pH. This is in a good agreement with the observed behavior of MB degradation for the titania coated on three types of substrates, where the best results were given at the highest pH.

In order to improve photocatalysts performance, different techniques have been used for increasing charge carriers concentration, charge separation and reducing the probability of electron-hole recombination, for instance, doping, morphology modification, and heterojunctions formation [53, 54].

In this work, sputtering technique was utilized to fabricate TiO₂ thin film on three substrate types (n-Si, p-Si and SiO₂). Semiconductor n-Si and p-Si are modified semiconductor which are fabricated by using doping method. The deposition of TiO₂ on the substrates can create heterojunction in the interface of substrate/TiO₂.

When combining two semiconductors occurs, a junction is created at the interface between the two semiconductors, where the difference position of the conduction band and the valence band will result in charge carrier transfer from one semiconductor to another, which subsequently increases charge separation and decreases the probability of electron-hole recombination. The decreasing of electron-hole recombination enhances the photocatalytic activity of catalyst.

Coronado [30] has given a brief illustration of the band edge position and band gap energy of some semiconductors, as reported in Figure 28.

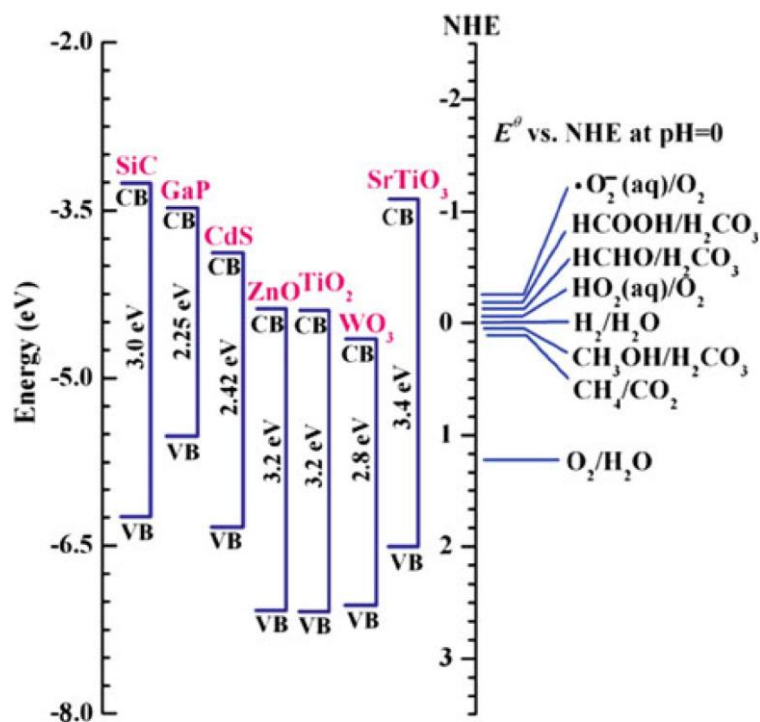


Figure 28. Band edge positions for various semiconductors in aqueous electrolyte at pH 0 [30]

TiO₂ is a n-type semiconductor [55] with band gap energy for anatase 3.2 eV [56], while silicon has band gap of 1.1 eV [31].

The Fermi level position of p-Si is close to the valence band. In contrast, the semiconductor n-Si has Fermi level position close to the conduction band. Hwang et al. [57] reported that the Fermi energy of n-Si is -4.25 eV and p-Si is -4.97 eV, relative to the vacuum level.

The Fermi level of n-type semiconductor TiO₂ can be calculated from the gap energy between the conduction band and the Fermi level which is can be calculated from equation (28) [58].

$$V_n = \frac{\kappa T}{q} \ln \left(\frac{N_C}{N_D} \right) \quad (28)$$

Where V_n is the gap energy between the conduction band and the Fermi level, κ is the Boltzmann constant ($1.38 \times 10^{-23} \text{ JK}^{-1}$), T is temperature (temperature measurement at 293 K), q is the charge of an electron (1.6×10^{-19}) [58]. N_C is the effective density of states in the conduction band, and it can be calculated by using equation (29) [58].

$$N_C = 2 \left(\frac{2\pi m_e^* \kappa T}{h^2} \right)^{\frac{3}{2}} \quad (29)$$

Where m_e^* is the electron effective mass ($m_e = 9.109 \times 10^{-31} \text{ kg}$ is the electron rest mass) and h is the Planck constant ($6.626 \times 10^{-34} \text{ Js}$)[58].

According to Hwang [57], the donor density (N_D) of TiO₂ is $2.76 \times 10^{17} \text{ cm}^{-3}$ and the electron effective mass of anatase (m_e^*) is equal to $1 m_e$. Based on those data, the calculated V_n of anatase is 0.81 eV. Then the Fermi level of TiO₂ can be predicted from the conduction band position of TiO₂ in Figure 28 and the calculated V_n of anatase.

The gap energy between the conduction band and the Fermi level of n-Si is 0.17 eV [58]. The conduction band position of n-Si can be calculated from V_n of n-Si and the reported Fermi level of n-Si.

In order to predict the the band bending that occurs in the semiconductor-semiconductor heterojunction, the knowledge of the band edge diagram is necessary. The calculated data and data from reference were collected to predict the band edge diagram of n-Si, p-Si and TiO₂ as follows.

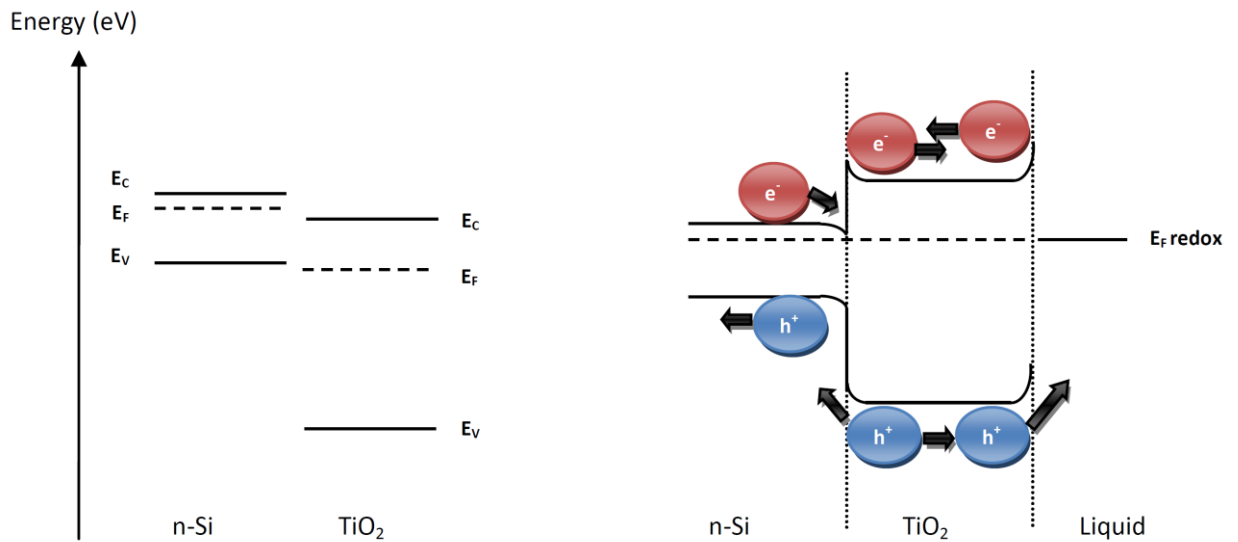


Figure 29. The band energies and charge transfer n-Si/TiO₂. Left side: before contact. Right side: after contact and UV light illumination.

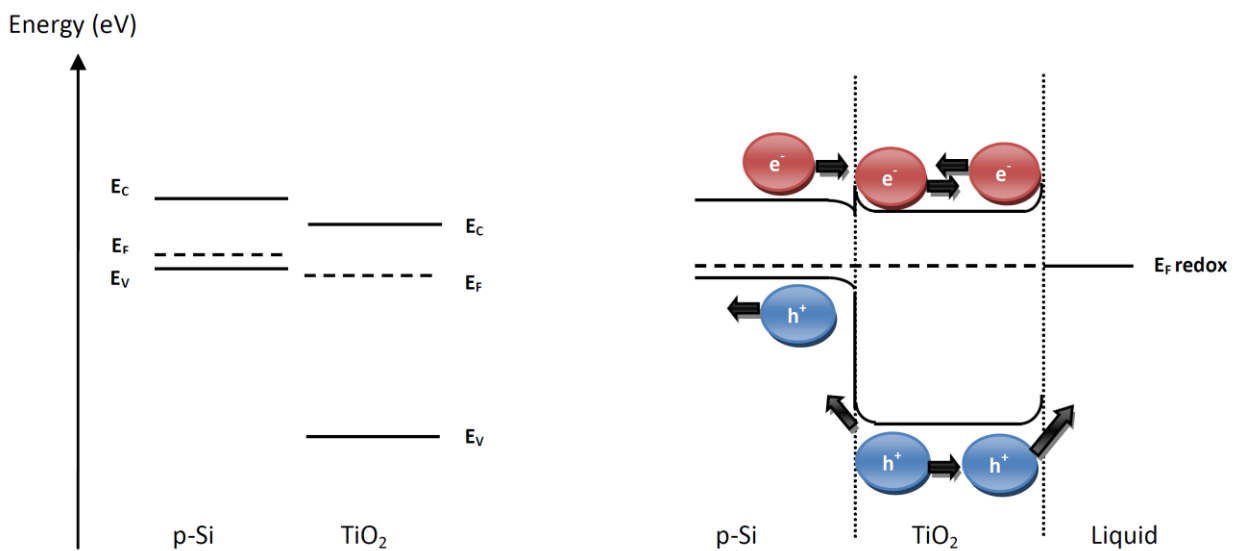


Figure 30. The band energies and charge transfer p-Si/TiO₂. Left side: before contact. Right side: after contact and UV light illumination.

In the semiconductors, combination between n-Si and TiO₂ can form n-Si/n-TiO₂ junction. As shown in Figure 29 (left side), before contact, the flat band energy level for n-Si and TiO₂ shows that the Fermi level of n-Si has significant gap with the Fermi level of TiO₂. When n-Si is contacted to TiO₂, the Fermi level of n-Si is shifted down and the Fermi level of TiO₂ is shifted up until it reaches equilibrium. This leads bands of n-type silicon, which is close to the interface of n-Si/TiO₂, to bend downward and bands of TiO₂ to bend upward. The band bending of the conduction band forms a well and a high barrier at the n-Si/TiO₂ junction, while the band bending of the valence band forms a jump at the n-Si/TiO₂ junction as illustrated in Figure 29 (right side).

When n-Si/TiO₂ system is contacted with liquid and illuminated with UV light, the electrons and holes are formed in both semiconductors as illustrated in Figure 29 (right side). The electrons in the conduction band of TiO₂ cannot be transferred to the liquid or the conduction band of n-Si because the band bending forms a high barrier [57]. The holes can migrate from the valence band of TiO₂ to the valence band of n-Si and to TiO₂/liquid interface until equilibrium state [55].

In the p-Si/TiO₂ system, the flat band energy level before contact is illustrated in Figure 30 (left side). The Fermi level of p-Si is slightly higher than the Fermi level of TiO₂. The Fermi level gap of p-Si/TiO₂ is smaller compared to n-Si/TiO₂ system. Figure 30 (right side) shows an illustration when p-Si is contacted to TiO₂, where the the Fermi level of n-Si is slightly shifted down and the Fermi level of TiO₂ is slightly shifted up until it is equal in equilibrium state. The bands of n-type silicon close to the interface of n-Si/TiO₂ will slightly bend downward and bands of TiO₂ will slightly bend upward. The band bending of the conduction band at the p-Si/TiO₂ junction also forms a well and a barrier, but it is lower than the barrier height of band bending at the n-Si/TiO₂ junction. The band bending of the valence band at the p-Si/TiO₂ junction has higher jump than at the n-Si/TiO₂ junction.

The p-Si/TiO₂ system is contacted with liquid and when it adsorbs photon, it generates electrons and holes in both side of the junction as illustrated in Figure 30 (right side). The electrons can be transferred from the conduction band of p-Si to TiO₂ because of low barrier at the p-Si/TiO₂ junction. The holes in the valence band of TiO₂ can migrate to the valence band of p-Si and the TiO₂/liquid interface. The migration of the electrons and holes increases the charge separation. Increase in charge separation reduces the electron-hole recombination, which results in an increase in photocatalysts performance of p-Si/TiO₂.

Silicon dioxide or SiO₂ is an insulator which has band gap energy of 9.2 eV [59]. In the SiO₂/TiO₂ system, when both of materials are contacted, there is no heterojunction formed between insulator and semiconductor. Therefore, when SiO₂/TiO₂ system was illuminated with UV light, there is no charge transfer between TiO₂ and SiO₂. The MB degradation by using SiO₂/TiO₂ system is based on the photocatalytic activity of TiO₂.

From the prediction of band energy and charge flow as above mentioned, theoretically the p-Si/TiO₂ system is likely has better photocatalytic performance than others because it has more charge separation which is decrease the electron-hole recombination. However, from the experiment results there is no significant MB degradation that can be used as evidence of the effect of substrate types on the photocatalytic performance.

4.4. Conclusions

The investigation of MB degradation by using titania thin film on different substrates (n-Si, p-Si and SiO₂) has been conducted. The observed photocatalytic MB degradation shows that there is no significant difference in the photocatalytic performance for the different substrate types. The highest photocatalytic performance of MB degradation is achieved at pH 9 due to the electrostatic attraction between negatively charged catalyst surface and cationic dye (MB). Additional hydroxyl radicals (OH^*) which are products of reaction between holes (h_{vb}^+) and surplus of hydroxide ions (OH^-) in the liquid phase at basic pH also increase the photocatalytic performance of titania layer at pH 9.

4.5. Recommendations

Based on this work, there was no significant different of MB degradation for different substrate types. Therefore, for future work, we need to modify the fabrication technique of titania layer in this work in order to improve the photocatalytic performance of TiO₂ such as changing substrate with metal and/or the addition of metal to TiO₂.

References

1. UN. Available from: <http://www.un.org/sustainabledevelopment/water-and-sanitation/>.
2. Robinson, T., et al., *Remediation of dyes in textile effluent: a critical review on current treatment technologies with a proposed alternative*. Bioresource Technology, 2001. **77**(3): p. 247-255.
3. Kasanen, J., et al., *Photocatalytic degradation of methylene blue in water solution by multilayer TiO₂ coating on HDPE*. Applied Surface Science, 2011. **258**(5): p. 1738-1743.
4. Gorges, R., S. Meyer, and G. Kreisel, *Photocatalysis in microreactors*. Journal of Photochemistry and Photobiology A: Chemistry, 2004. **167**(2–3): p. 95-99.
5. Goetz, V., et al., *Modeling aqueous heterogeneous photocatalytic degradation of organic pollutants with immobilized TiO₂*. Chemical Engineering and Processing: Process Intensification, 2009. **48**(1): p. 532-537.
6. Aran, H.C., et al., *Porous Photocatalytic Membrane Microreactor (P2M2): A new reactor concept for photochemistry*. Journal of Photochemistry and Photobiology A: Chemistry, 2011. **225**(1): p. 36-41.
7. Dijkstra, M.F.J., et al., *Modeling the photocatalytic degradation of formic acid in a reactor with immobilized catalyst*. Chemical Engineering Science, 2002. **57**(22–23): p. 4895-4907.
8. Amy L. Linsebigler, G.L., John T. Yates, *Photocatalysis on TiO₂ Surfaces: Principles, Mechanisms, and Selected*. Chem. Rev, 1995. **95**: p. 735-759.
9. Herrmann, J.-M., *Heterogeneous photocatalysis: fundamentals and applications to the removal of various types of aqueous pollutants*. Catalysis Today, 1999. **53**(1): p. 115-129.
10. Parvaneh Sangpour, F.H., Alireza Z. Moshfegh, *Photoenhanced Degradation of Methylene Blue on Cosputtered M: TiO₂ (M = Au, Ag, Cu) Nanocomposite systems: a Comparative Study*. J. Phys. Chem., 2010. **114**: p. 13955-13961.
11. Chong, M.N., et al., *Recent developments in photocatalytic water treatment technology: A review*. Water Research, 2010. **44**(10): p. 2997-3027.
12. Gaya, U.I. and A.H. Abdullah, *Heterogeneous photocatalytic degradation of organic contaminants over titanium dioxide: A review of fundamentals, progress and problems*. Journal of Photochemistry and Photobiology C: Photochemistry Reviews, 2008. **9**(1): p. 1-12.
13. Jenks, W.S., *Photocatalytic Reaction Pathways – Effects of Molecular Structure, Catalyst, and Wavelength*, in *Photocatalysis and Water Purification*. 2013, Wiley-VCH Verlag GmbH & Co. KGaA. p. 25-51.
14. Nakata, K. and A. Fujishima, *TiO₂ photocatalysis: Design and applications*. Journal of Photochemistry and Photobiology C: Photochemistry Reviews, 2012. **13**(3): p. 169-189.
15. Yamagishi, M., et al., *Thin film TiO₂ photocatalyst deposited by reactive magnetron sputtering*. Thin Solid Films, 2003. **442**(1–2): p. 227-231.
16. Kim, S.B. and S.C. Hong, *Kinetic study for photocatalytic degradation of volatile organic compounds in air using thin film TiO₂ photocatalyst*. Applied Catalysis B: Environmental, 2002. **35**(4): p. 305-315.
17. Anitha, V.C., A.N. Banerjee, and S.W. Joo, *Recent developments in TiO₂ as n- and p-type transparent semiconductors: synthesis, modification, properties, and energy-related applications*. Journal of Materials Science, 2015. **50**(23): p. 7495-7536.
18. Natarajan, K., et al., *Photocatalytic reactor based on UV-LED/TiO₂ coated quartz tube for degradation of dyes*. Chemical Engineering Journal, 2011. **178**: p. 40-49.
19. Ahmed, S., et al., *Influence of parameters on the heterogeneous photocatalytic degradation of pesticides and phenolic contaminants in wastewater: A short review*. Journal of Environmental Management, 2011. **92**(3): p. 311-330.

20. Charles, G., et al., *Determination of kinetic constants of a photocatalytic reaction in micro-channel reactors in the presence of mass-transfer limitation and axial dispersion*. Journal of Photochemistry and Photobiology A: Chemistry, 2011. **223**(2–3): p. 202-211.
21. Assadi, A.A., A. Bouzaza, and D. Wolbert, *Photocatalytic oxidation of trimethylamine and isovaleraldehyde in an annular reactor: Influence of the mass transfer and the relative humidity*. Journal of Photochemistry and Photobiology A: Chemistry, 2012. **236**: p. 61-69.
22. Imoberdorf, G.E., et al., *Scaling-up from first principles of a photocatalytic reactor for air pollution remediation*. Chemical Engineering Science, 2007. **62**(3): p. 793-804.
23. Ratova, M., et al., *Enhanced properties of magnetron sputtered photocatalytic coatings via transition metal doping*. Surface and Coatings Technology, 2013. **228, Supplement 1**: p. S544-S549.
24. Suda, Y., et al., *Preparation of high quality nitrogen doped TiO₂ thin film as a photocatalyst using a pulsed laser deposition method*. Thin Solid Films, 2004. **453–454**: p. 162-166.
25. Gora, S.L. and S.A. Andrews, *Adsorption of natural organic matter and disinfection byproduct precursors from surface water onto TiO₂ nanoparticles: pH effects, isotherm modelling and implications for using TiO₂ for drinking water treatment*. Chemosphere, 2017. **174**: p. 363-370.
26. Chiu, S.-M., et al., *Photocatalytic activity of doped TiO₂ coatings prepared by sputtering deposition*. Journal of Materials Processing Technology, 2007. **192–193**: p. 60-67.
27. Pihosh, Y., et al., *Photocatalytic property of TiO₂ thin films sputtered-deposited on unheated substrates*. Applied Surface Science, 2009. **256**(4): p. 937-942.
28. Hanaor, D.A.H. and C.C. Sorrell, *Review of the anatase to rutile phase transformation*. Journal of Materials Science, 2011. **46**(4): p. 855-874.
29. Zhang, J., et al., *New understanding of the difference of photocatalytic activity among anatase, rutile and brookite TiO₂*. Physical Chemistry Chemical Physics, 2014. **16**(38): p. 20382-20386.
30. Coronado, J.M., *Photons, Electrons and Holes: Fundamentals of Photocatalysis with Semiconductors*, in *Design of Advanced Photocatalytic Materials for Energy and Environmental Applications*, J.M. Coronado, et al., Editors. 2013, Springer London: London. p. 5-33.
31. Vincenzo Augugliaro, V.L., Mario Pagliaro, Giovanni Palmisano, Leonardo Palmisano, *Clean by Light Irradiation : Practical Applications of Supported TiO₂*. 2011.
32. Smith, R.E. and S. Updated by, *Azine Dyes*, in *Kirk-Othmer Encyclopedia of Chemical Technology*. 2000, John Wiley & Sons, Inc.
33. Ginimuge, P. and S. Jyothi, *Methylene blue: Revisited*. Journal of Anaesthesiology Clinical Pharmacology, 2010. **26**(4): p. 517-520.
34. Berneth, H., *Cationic Dyes*, in *Ullmann's Encyclopedia of Industrial Chemistry*. 2000, Wiley-VCH Verlag GmbH & Co. KGaA.
35. ; Available from: https://pubchem.ncbi.nlm.nih.gov/compound/methylene_blue#section=Top.
36. Sajid Ullah, K. and E.t.E. Johan, *Patterning titania with the conventional and modified micromolding in capillaries technique from sol–gel and dispersion solutions*. Science and Technology of Advanced Materials, 2012. **13**(2): p. 025002.
37. Huang, C.-C., et al., *A well-dispersed catalyst on porous silicon micro-reformer for enhancing adhesion in the catalyst-coating process*. International Journal of Hydrogen Energy, 2014. **39**(15): p. 7753-7764.
38. Stefanescu, A., et al., *Wall coating optimization for microchannel reactors*. Catalysis Today, 2007. **125**(1–2): p. 16-23.

39. D'Angelo, M.F.N., et al., *Hydrogen Production through Aqueous-Phase Reforming of Ethylene Glycol in a Washcoated Microchannel*. *ChemSusChem*, 2013. **6**(9): p. 1708-1716.
40. Liu, M., J. Sun, and Q. Chen, *Influences of heating temperature on mechanical properties of polydimethylsiloxane*. *Sensors and Actuators A: Physical*, 2009. **151**(1): p. 42-45.
41. Taylor, G., *Deposition of a viscous fluid on the wall of a tube*. *Journal of Fluid Mechanics*, 1961. **10**(2): p. 161-165.
42. Deng, Y. and R. Zhao, *Advanced Oxidation Processes (AOPs) in Wastewater Treatment*. *Current Pollution Reports*, 2015. **1**(3): p. 167-176.
43. Satuf, M.L., et al., *Kinetic modeling of azo dyes photocatalytic degradation in aqueous TiO₂ suspensions. Toxicity and biodegradability evaluation*. *Catalysis Today*, 2011. **161**(1): p. 121-126.
44. Visan, A., *Modeling intrinsic kinetics in immobilized photocatalytic microreactors*. 2015, University of Twente.
45. Stefanov, B.I., et al., *Novel integrated reactor for evaluation of activity of supported photocatalytic thin films: Case of methylene blue degradation on TiO₂ and nickel modified TiO₂ under UV and visible light*. *Colloids and Surfaces A: Physicochemical and Engineering Aspects*, 2011. **382**(1-3): p. 219-225.
46. Damon Rafieian, R.T.D., Wojciech Ogieglo, Rob G.H. Lammertink, *Intrinsic Photocatalytic Assessment of Reactively Sputtered TiO₂ Films*. *ACS Appl. Mater. Interfaces*, 2015. **7**: p. 8727-8732.
47. Chou, J.-C. and L.P. Liao, *Study on pH at the point of zero charge of TiO₂ pH ion-sensitive field effect transistor made by the sputtering method*. *Thin Solid Films*, 2005. **476**(1): p. 157-161.
48. Zhu, X., et al., *Photocatalytic degradation of pesticide pyridaben on TiO₂ particles*. *Journal of Molecular Catalysis A: Chemical*, 2005. **229**(1-2): p. 95-105.
49. Coronado, J.M. and M.D. Hernández-Alonso, *The Keys of Success: TiO₂ as a Benchmark Photocatalyst*, in *Design of Advanced Photocatalytic Materials for Energy and Environmental Applications*, J.M. Coronado, et al., Editors. 2013, Springer London: London. p. 85-101.
50. Shahrezaei, F., et al., *Process modeling and kinetic evaluation of petroleum refinery wastewater treatment in a photocatalytic reactor using TiO₂ nanoparticles*. *Powder Technology*, 2012. **221**: p. 203-212.
51. Houas, A., et al., *Photocatalytic degradation pathway of methylene blue in water*. *Applied Catalysis B: Environmental*, 2001. **31**(2): p. 145-157.
52. Kushwaha, A.K., N. Gupta, and M.C. Chattopadhyaya, *Removal of cationic methylene blue and malachite green dyes from aqueous solution by waste materials of *Daucus carota**. *Journal of Saudi Chemical Society*, 2014. **18**(3): p. 200-207.
53. Zhang, L. and M. Jaroniec, *Toward designing semiconductor-semiconductor heterojunctions for photocatalytic applications*. *Applied Surface Science*, 2017.
54. Chen, X., et al., *Semiconductor-based Photocatalytic Hydrogen Generation*. *Chemical Reviews*, 2010. **110**(11): p. 6503-6570.
55. Scuderi, V., et al., *TiO₂ coated CuO nanowire array: Ultrathin p-n heterojunction to modulate cationic/anionic dye photo-degradation in water*. *Applied Surface Science*, 2017. **416**: p. 885-890.
56. Rafieian, D., *Catalytic water cleaning: materials and transport aspects*, in *Department of Science and Technology*. 2016, University of Twente.
57. Hwang, Y.J., A. Boukai, and P. Yang, *High Density n-Si/n-TiO₂ Core/Shell Nanowire Arrays with Enhanced Photoactivity*. *Nano Letters*, 2009. **9**(1): p. 410-415.

58. Yao, T., et al., *Manipulating the Interfacial Energetics of n-type Silicon Photoanode for Efficient Water Oxidation*. *Journal of the American Chemical Society*, 2016. **138**(41): p. 13664-13672.
59. Kamat, P.V., *Manipulation of Charge Transfer Across Semiconductor Interface. A Criterion That Cannot Be Ignored in Photocatalyst Design*. *The Journal of Physical Chemistry Letters*, 2012. **3**(5): p. 663-672.